

# Time-delayed beam splitting with energy separation of x-ray channels

Yuri P. Stetsko,<sup>1</sup> Yuri V. Shvyd'ko,<sup>1,\*</sup> and G. Brian Stephenson<sup>1</sup>

<sup>1</sup>*Advanced Photon Source, Argonne National Laboratory, Argonne, Illinois 60439, USA*

We introduce a time-delayed beam splitting method based on the energy separation of x-ray photon beams. It is implemented and theoretically substantiated on an example of an x-ray optical scheme similar to that of the classical Michelson interferometer. The splitter/mixer uses Bragg-case diffraction from a thin diamond crystal. Another two diamond crystals are used as back-reflectors. For energy separation the back-reflectors are set at slightly different temperatures and angular deviations from exact backscattering. Because of energy separation and a minimal number (three) of optical elements, the split-delay line has high efficiency and is simple to operate. Due to the high transparency of diamond crystal, the split-delay line can be used in a beam sharing mode at x-ray free-electron laser facilities. The delay line can be made more compact by adding a fourth crystal.

PACS numbers: 41.50.+h, 07.85.Nc, 78.70.Ck, 61.05.C-

Complex nanoscale dynamics in condensed matter can be studied in a broad dynamic range by x-ray photon correlation spectroscopy (XPCS) using coherent x-rays from x-ray free-electron lasers (XFELs) [1]. The split-pulse technique is one of the promising approaches to access dynamics from femtosecond to nanosecond regimes. In this technique, each x-ray pulse is split into reference and delayed pulses of equal intensity, arriving at the sample separated in time. The scattering from the reference and delayed pulses is then collected during the same exposure of an area detector.

The principle optical scheme of the split-pulse technique was discussed in [1–3]. The main components are a splitter and mixer crystals in Bragg diffraction, and two additional Bragg reflecting crystals guiding the delayed pulse and controlling the delay. To ensure very short (femtosecond length) and even negative delays, an advanced scheme was proposed and realized [4–6]. It has additional four crystals (total eight) designed to guide the reference pulse. The large number of optical elements inevitably complicates alignment and operations, and also compromises the split-delay line efficiency.

Here we introduce and study theoretically the performance of a split-delay x-ray scheme with the minimal amount of crystals, three, as shown in Fig. 1. The scheme resembles the classical Michelson interferometer [24]. Crystal  $C_0$  plays the roles of both the splitter and the mixer. Crystals  $C_2$  and  $C_1$  are set to reflect x-rays in almost exact Bragg backscattering geometry, and guide the reference (red) and delayed (blue) pulses to sample  $S$  through  $C_0$  or by reflecting from  $C_0$ , respectively. The delay  $\tau = 2L/c$  is varied by changing the crystal  $C_2$  spatial position along the beam, i.e., a delay path  $L$ .

The central problem in the design of a split-delay line is how to split the incident beam and how to bring together the reference and delayed beams on the sample. In the traditional scheme, which we term as single-energy splitting (SES), photons of the same energy are divided

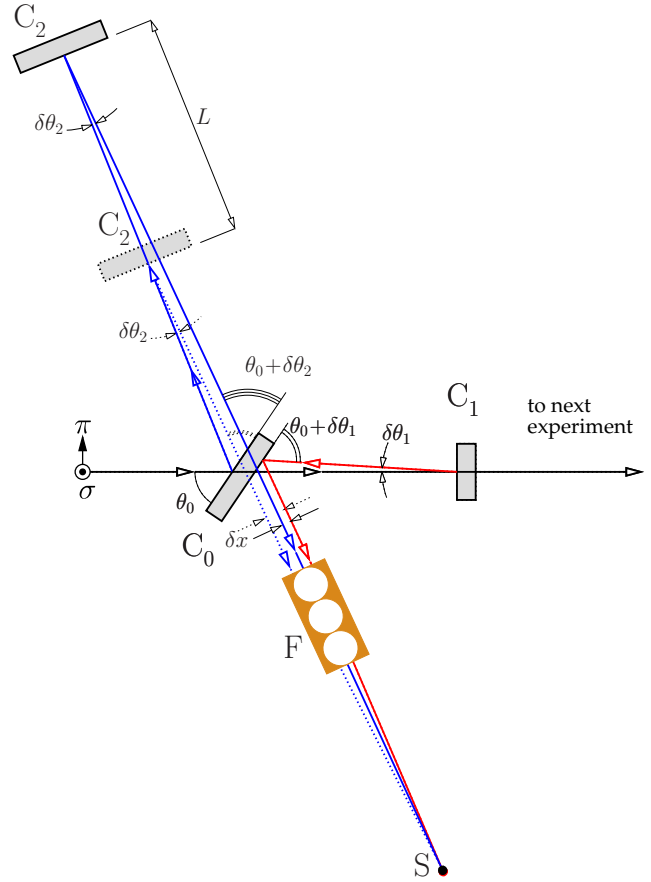


FIG. 1: Optical scheme of a three-crystal  $C_0$ ,  $C_1$ ,  $C_2$ , split-delay line in a Michelson-interferometer-type configuration using dual-energy splitting (see text for details). The reference (red) and delayed (blue) beams are shifted parallel to each other by  $\delta x$ , provided the angular deviations from exact backscattering  $\delta\theta_1 = \delta\theta_2$ . The parallel beams are focused on sample  $S$  by focusing system  $F$ . The shift  $\delta x$ , see Eq. (1), is due to a finite thickness  $d$  of crystal  $C_0$ , and a delay path length  $L$  determining the nonzero x-ray pulse delay  $\tau = 2L/c$ .

between the reference and delayed beams. Equal intensity splitting can be realized by using Bragg diffraction

\*Electronic address: shvydtko@aps.anl.gov

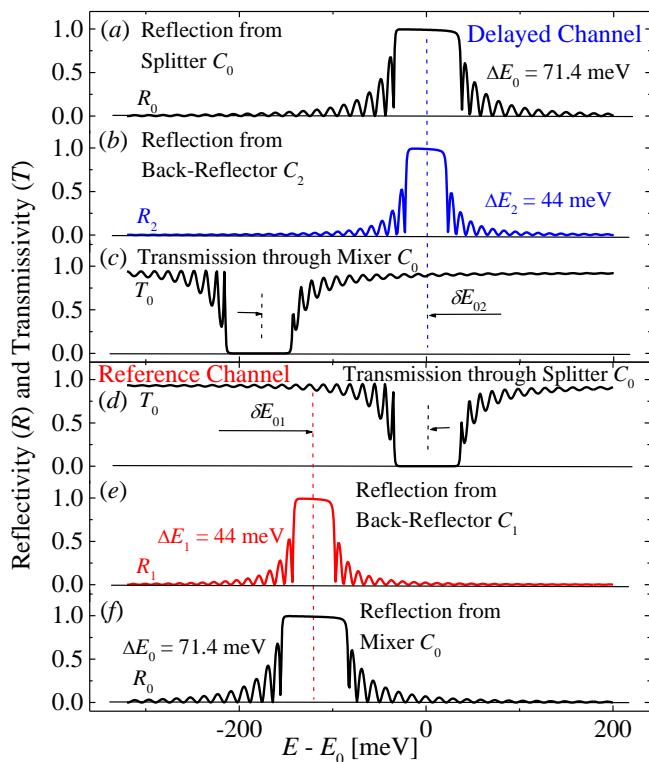


FIG. 2: Spectral dependencies of reflection (R) from and transmission (T) through individual crystals of the split-delay line, calculated in the framework of the dynamical theory of x-ray diffraction, with crystal parameters of device 1, given in Table I.

in the reflection (Bragg-case) geometry. To transmit 50% of the incident beam into the forward direction, crystal thickness should be close to the extinction length  $\Lambda$ . For suitable Bragg reflections in silicon, diamond, and some other crystals,  $\Lambda \approx 1 - 10 \mu\text{m}$ , which requires very thin crystals, the manufacture of which is a challenging but now feasible task [7]. Alternatively, Bragg diffraction in the transmission (Laue-case) geometry can be used. The thicknesses of the splitter has to be chosen as an integer of the Pendellösung length, which is closely related to  $\Lambda$  [8]. Also in this case, equal intensity splitting can be realized; however, one should be aware of the following potential problems. First, the intensity between the two channels is very sensitive to thickness errors. Second, the angular acceptance of the splitter as well as the beams intensities sufficiently decrease with increasing crystal thickness.

In the present Letter we study a beam splitting method based on the photon energy separation of x-ray beams, which we refer to here as dual-energy splitting (DES) [25]. DES is implemented here and studied theoretically on the example of the x-ray Michelson-interferometer-type optical scheme, as shown in Fig. 1, and briefly presented above. A few more details regarding the scheme are in order.

The splitter/mixer crystal  $C_0$  reflects x-ray photons in an energy bandwidth  $\Delta E_0$  into the delayed pulse chan-

nel, shown in blue in Fig. 1. The reflectivity is close to 100% if the crystal thickness  $d \gg \Lambda$ , see Fig. 2(a). The incidence angle  $\theta_0$  is such that the central photon energy  $E_0$  of the spectral distribution coincides with the central energy  $E_2$  of the reflection bandwidth from crystal  $C_2$  set into backscattering, see Fig. 2(b). The bandwidth  $\Delta E_2$  of crystal  $C_2$  is chosen to be close to the bandwidth  $\Delta E_0$  of crystal  $C_0$ . The x-rays back-reflected from  $C_2$  are transmitted through  $C_0$  and steered onto the sample S, provided the angular offset  $\delta\theta_2$  is larger than the angular width  $\Delta\theta_0 = (\Delta E_0/E_0) \tan \theta_0$  of the Bragg reflection from  $C_0$ . This can be easily realized, since the angular width of back-reflection  $\Delta\theta_2 = 2\sqrt{\Delta E_2/E_2}$  is much larger [9, 10].

X-ray photons with energies outside the energy bandwidth  $\Delta E_0$  are transmitted through  $C_0$ , see Fig. 2(d), and guided into the reference pulse channel by back reflection from  $C_1$ , as shown in red in Fig. 1. Crystal  $C_1$  is equivalent to  $C_2$ . However, it is maintained at a different temperature  $T_1 = T_2 + \delta T_{12}$  to reflect x-rays transmitted through  $C_0$  in a bandwidth centered at  $E_1$ , which is shifted from  $E_2$  by  $\delta E_{01} = E_0 - E_1 > (\Delta E_0 + \Delta E_1)/2$ , see Fig. 2(e). Photons back-reflected from  $C_1$  will be reflected from  $C_0$ , see Fig. 2(f), and directed onto the sample, provided the angle of incidence to  $C_0$  is  $\theta_0 + \delta\theta_1$ , where according to Bragg's law  $\delta\theta_1 = (\delta E_{01}/E_0) \tan \theta_0$ . The same angular deviation  $\delta\theta_1$  is required in backscattering from  $C_1$ , see Fig. 1.

If  $\delta\theta_1 = \delta\theta_2$ , the two beams propagate to the sample parallel to each other with a small offset

$$\delta x = 2d_0 \cos \theta_0 - L \delta\theta_1. \quad (1)$$

For  $d_0 = 50 \mu\text{m}$  the first term in Eq. (1) is about  $60 \mu\text{m}$ , while the second term varies from zero for  $L = 0$  to  $-30 \mu\text{m}$  for  $L = 1.5 \text{ m}$ . As a result,  $\delta x$  varies from  $60 \mu\text{m}$  to  $30 \mu\text{m}$ , respectively. Given, a usual XFEL beam size of  $\simeq 300 - 700 \mu\text{m}$ , such shift is insignificant. Despite the shift, focusing system F brings all the photons to the same point on the sample.

Spectral dependencies of reflection from and transmission through each crystal optical element of the split-delay line are presented in Fig. 2, numerically calculated according to [11] using equations of the dynamical theory of x-ray diffraction. Spectral distribution of x-rays arriving on the sample in the reference and delayed channels are shown in Fig. 3(a) by the red and blue lines, respectively. The calculations are performed assuming that the XFEL is working in a self-seeding mode providing x-rays in a 400-meV bandwidth (black line) [12], and with an angular spread of  $2.5 \mu\text{rad}$  (FWHM).

The calculations presented in Figs. 2 and 3, are performed with crystal parameters given in Table I for device 1. The choice of the crystals is not unique. In this particular example, diamond crystals are chosen for all three optical elements for several reasons. First, the photoabsorption in diamond is much less than in Si, and therefore the efficiency of diamond optics is higher. Second, for the same photon energy, the spectral bandwidth of

device #	polarization	crystal $C_n$	material	$(hkl)$	$T_n$ [K]	$E_n$ [keV]	$\Delta E_n$ [meV]	$\theta_n$	$\Delta\theta_n$ [ $\mu$ rad]	$d_n$ [ $\mu$ m]	$\varepsilon_n$ %	$\varepsilon_n^{(abs)}$ %
1	$\sigma$	$C_0$	diamond	(004)	300	8.51389	72	$54.7359^\circ$	12	50	–	–
		$C_1$	diamond	(224)	$T_2 + \delta T_{12}$ $\delta T_{12}=13$ K	$E_0 - \delta E_{01}$ $\delta E_{01}=120$ meV	44	$90^\circ - \delta\theta_1/2$ $\delta\theta_1=20$ $\mu$ rad	3675	50	94	9.9
		$C_2$	diamond	(224)	300	$E_0$	44	$90^\circ - \delta\theta_2/2$	3675	50	93	9.8
		$C_3$	diamond	(220)	300	$E_0$	176	$90^\circ - \theta_0$	15	>50	–	–
2	$\pi$	$C_0$	diamond	(220)	300	8.51389	66	$35.2641^\circ$	5.5	50	–	–
		$C_1$	diamond	(224)	$T_2 + \delta T_{12}$ $\delta T_{12}=13$ K	$E_0 - \delta E_{01}$ $\delta E_{01}=120$ meV	44	$90^\circ - \delta\theta_1/2$ $\delta\theta_1=10$ $\mu$ rad	3675	50	85	8.6
		$C_2$	diamond	(224)	300	$E_0$	44	$90^\circ - \delta\theta_2/2$	3675	50	84	8.5

TABLE I: Crystal elements  $C_n$  ( $n = 0, 1, 2$ ) of two split-delay lines schematically presented in Fig. 1, and  $C_n$  ( $n = 0, 1, 2, 3$ ) of the split-delay lines schematically presented in Fig. 4. Crystal, Bragg reflection parameters, and incident radiation polarization states are given as used in all dynamical theory calculations:  $(hkl)$  - Miller indices of Bragg reflections;  $T_n$  - crystal temperature,  $d_n$  - crystal thickness,  $\theta_n$  - glancing angle of incidence;  $E_n$  - photon energy at the reflection curve center;  $\Delta E_n$ , and  $\Delta\theta_n$  are Bragg's reflection spectral width, and angular acceptance, respectively.  $\varepsilon_n$  and  $\varepsilon_n^{(abs)}$  are the relative and absolute efficiencies of respective channels.

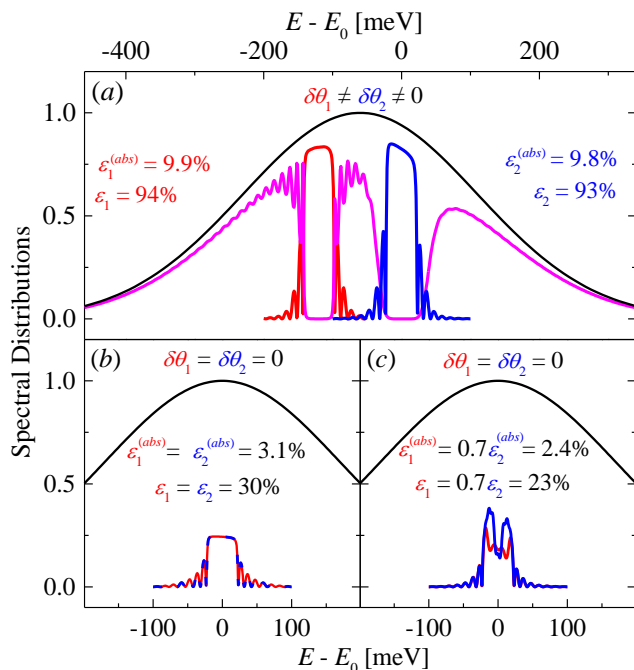


FIG. 3: Spectral distribution of x-rays arriving on the sample in the reference (red line) and delayed (blue line) channels, calculated using the dynamical theory of x-ray diffraction, with crystal parameters of device 1, given in Table I. Black line shows the spectrum of incident x-rays from a seeded XFEL. The magenta line shows the spectral distribution of the photons, transmitted through crystals  $C_0$  and  $C_1$ . (a) Calculations for the dual-energy splitting case. (b)-(c) Calculations under similar conditions, but with  $C_0$  functioning in the single-energy splitting mode in Bragg-case and Laue-case diffractions, respectively.

Bragg back-reflections from diamond crystals is larger,

due to larger Debye-Waller factors (larger Debye temperature) [13, 14]. We have chosen Bragg reflections with the largest bandwidth and therefore with the highest efficiency, applicable in a comfortable for XPCS experiments photon range of 8-9 keV. Given the very recent advancement in fabrication of high-quality diamond crystals and their use in high-resolution, low-loss x-ray optics [12, 14–17], the proposed configuration with diamond crystal elements is deemed to be feasible.

Bragg back-reflection is very often accompanied by parasitic Bragg reflections [10, 18–20], which may waste a significant number of useful photons and reduce the optics efficiency. The choice of back-reflection was actually dictated also by the requirement of the minimal amount of the parasitic reflections. In particular, the 422 back-reflection from  $C_1$  and  $C_2$  diamond crystals considered here is accompanied only by one pair of the parasitic Bragg reflections: 400 and 022. It is easy to suppress them. To do this, the crystal plane containing the (422), (400), and (022) reciprocal vectors has to be inclined by  $\simeq 100$   $\mu$ rad to the 422 Bragg diffraction plane.

Efficiency is a figure of merit for a split-delay line. Relative spectral efficiencies for the reference and delayed channels are very high:  $\varepsilon_1 \simeq 94\%$  and  $\varepsilon_2 \simeq 93\%$ , respectively. The relative spectral efficiency is defined as the number of photons in the relevant channel normalized to the number of incident photons within the channel bandwidth. Absolute spectral efficiencies are calculated by normalization to the total number of incident photons. For the 400-meV bandwidth of the XFEL radiation, they are equal to  $\varepsilon_1^{(abs)} = 9.9\%$  and  $\varepsilon_2^{(abs)} = 9.8\%$ , respectively. The total absolute efficiency of the scheme is about 20%. The rest of the photons,  $\simeq 60\%$ , transmitted through both  $C_0$  and  $C_1$  can be utilized by the downstream experiment. Therefore, such a split-delay line can be used in a beam sharing mode at XFEL facilities.

Figures 3(b) and 3(c) show for comparison the results

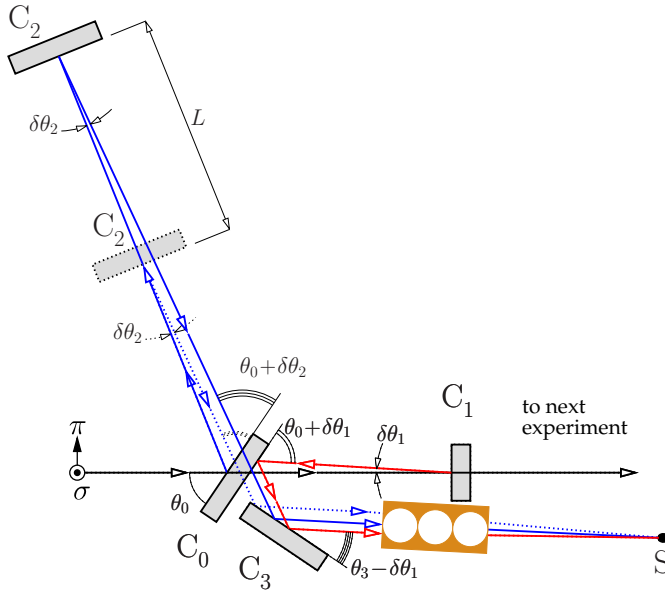


FIG. 4: By adding crystal  $C_3$  with  $\theta_3 = \pi/2 - \theta_0$  the delay line in Fig. 1 becomes more compact, with reference and delayed pulses propagating almost parallel to the incident beam.

of calculations of the spectral distributions for the same scheme, but, with  $C_0$  functioning in single-energy splitting mode in Bragg-case (b) or Laue-case (c) diffraction, with  $d_0 = 6.4 \mu\text{m}$  and  $d_0 = 52.4 \mu\text{m}$ , respectively. Single-energy splitting requires that  $\delta\theta_2 = \delta\theta_1 = 0$ . The values of efficiencies indicated in Fig. 3 show that the dual-energy splitting scheme is about three to four times more efficient than the single-energy splitting schemes.

If the vertical configuration is inconvenient, the same scheme could be used in the horizontal scattering geometry. In this case the incident radiation is in the  $\pi$ -polarization state. Device 2 in Table I presents an example of the split-delay line functioning in horizontal scattering plane and having very similar performance in terms of efficiency and other parameters.

The scheme could be made more compact, with the beams propagating to the sample parallel to the incident beam. This is achieved by additional Bragg reflection from an additional crystal  $C_3$  with Bragg angle  $\theta_3 = \pi/2 - \theta_0$ , as shown in Fig. 4. The efficiency of the four-crystal scheme is almost the same as that of the three-crystal scheme, provided a high-reflectivity diamond crystal  $C_3$  is used, as suggested in Table I.

The split-delay lines presented here are also applicable at synchrotron radiation facilities. The larger angular divergence of the incident beam  $\simeq 10 - 15 \mu\text{rad}$  will, however, result in a  $\simeq 15 - 30\%$  reduction of the efficiency for the three-crystal scheme and a  $\simeq 20 - 35\%$  reduction of the efficiency for the four-crystal scheme.

In conclusion, the three-crystal split-delay x-ray scheme for XPCS applications is introduced and studied theoretically. Application of the dual-energy splitting significantly increases the efficiency of the optical scheme. Due to the high transparency of diamond crystal, the split-delay line of such design can be used at XFEL facilities in the beam sharing mode. A four-crystal modification makes the scheme in-line and more convenient for XPCS experiments.

Work was supported by the U.S. Department of Energy, Office of Science, under Contract No. DE-AC02-06CH11357.

- [1] G. Grüberl, G. B. Stephenson, C. Gutt, H. Sinn, and T. Tschentscher, Nucl. Instrum. Methods Phys. Res. B **252**, 357367 (2007).
- [2] G. Materlik and T. Tschentscher, eds., *TESLA. The superconducting Electron-Positron Linear Collider with an Integrated X-ray Laser Laboratory. Part V, The X-Ray Free Electron Laser* (DESY, Hamburg, 2001).
- [3] M. Altarelli, R. Brinkmann, M. Chergui, W. Decking, B. Dobson, S. Dusterer, G. Grüberl, W. Graeff, H. Graafsma, J. Hajdu, et al., *XFEL: The European X-Ray Free-Electron Laser : Technical design report* (DESY, Hamburg, 2006).
- [4] Conceptual Design Report for the Linac Coherent Light Source, Tech. Rep. SLAC-R-593, SLAC (2002).
- [5] W. Roseker, H. Franz, H. Schulte-Schrepping, A. Ehnes, O. Leupold, F. Zontone, A. Robert, and G. Grüberl, Optics Letters **34**, 1768 (2009).
- [6] W. Roseker, H. Franz, H. Schulte-Schrepping, A. Ehnes, O. Leupold, F. Zontone, S. Lee, A. Robert, and G. Grüberl, J. Synchrotron Radiation **18**, 481 (2011).
- [7] T. Osaka, M. Yabashi, Y. Sano, K. Tono, Y. Inubushi, T. Sato, S. Matsuyama, T. Ishikawa, and K. Yamauchi, Optics Express **21**, 2823 (2013).
- [8] A. Authier, *Dynamical Theory of X-Ray Diffraction*, vol. 11 of *IUCr Monographs on Crystallography* (Oxford University Press, Oxford, New York, 2001).
- [9] K. Kohra and T. Matsushita, Z. Naturforsch. A **27**, 484 (1972).
- [10] Y. Shvyd'ko, *X-Ray Optics - High-Energy-Resolution Applications*, vol. 98 of *Optical Sciences* (Springer, Berlin Heidelberg New York, 2004).
- [11] Y. P. Stetsko and S.-L. Chang, Acta Cryst. **A53**, 28 (1997).
- [12] J. Amann, W. Berg, V. Blank, F.-J. Decker, Y. Ding, P. Emma, Y. Feng, J. Frisch, D. Fritz, J. Hastings, et al., Nature Photonics **6** (2012).
- [13] Y. V. Shvyd'ko, S. Stoupin, A. Cunsolo, A. Said, and X. Huang, Nature Physics **6**, 196 (2010).
- [14] Y. V. Shvyd'ko, S. Stoupin, V. Blank, and S. Terentyev, Nature Photonics **5**, 539 (2011).
- [15] S. Polyakov, V. Denisov, N. Kuzmin, M. Kuznetsov, S. Martyushov, S. Nosukhin, S. Terentiev, and V. Blank, Diamond and Related Materials **20**, 726 (2011).
- [16] S. Stoupin, V. Blank, S. Terentyev, S. Polyakov, V. Denisov, M. Kuznetsov, Y. Shvyd'ko, D. Shu, P. Emma, J. Maj, et al., Diamond and Related Mate-

- rials **33**, 1 (2013).
- [17] R. C. Burns, A. I. Chumakov, S. H. Connell, D. Dube, H. P. Godfried, J. O. Hansen, J. Härtwig, J. Hozzowska, F. Masiello, L. Mkhonza, et al., *J. Phys.: Condensed Matter* **21**, 364224(14pp) (2009).
- [18] J. P. Sutter, E. E. Alp, M. Y. Hu, P. L. Lee, H. Sinn, W. Sturhahn, T. S. Toellner, G. Bortel, and R. Collela, *Phys. Rev. B* **63**, 094111 (2001).
- [19] M. Lerche and Y. V. Shvyd'ko, *Phys. Rev. B* **70**, 134104 (2004).
- [20] M. S. Chiu, Y. P. Stetsko, and S.-L. Chang, *Acta Crystallographica A* **64**, 394 (2008).
- [21] A. Appel and U. Bonse, *Phys. Rev. Lett.* **67**, 1673 (1991).
- [22] M. Nusshardt and U. Bonse, *J. Appl. Cryst.* **36**, 269 (2003).
- [23] J. P. Sutter, T. Ishikawa, U. Kuetgens, G. Materlik, Y. Nishino, A. Rostomyan, K. Tamasaku, and M. Yabashi, *Journal of Synchrotron Radiation* **11**, 378 (2004).
- [24] We note here that an x-ray version of the Michelson interferometer, designed for hard x-ray Fourier spectroscopy applications, was already implemented in hard x-ray optics; however, it used many (eight) crystals and Bragg reflections in far from exact backscattering conditions [21–23].
- [25] While working on the manuscript, it came to our attention that a similar idea of energy separation of the x-ray beams has been discussed in [7] for a very thin splitter without performing theoretical analysis or experiments.